5

Micro-Fabrication of Planar Inductors for High Frequency DC-DC Power Converters

Elias Haddad, Christian Martin, Bruno Allard,
Maher Soueidan and Charles Joubert
Université de Lyon, Université Lyon 1,
CNRS UMR5005 AMPERE,
France

1. Introduction

The inductors are essential elements for radiofrequency (RF) integrated circuits. A large number of communication devices functioning in RF such as mobile phones or wireless ethernet require transceivers, filters and power amplifiers in which inductors are critical components. Recently, the push toward miniaturisation of electronic components enabled to embark more and more portable equipments and accessories of high energy consumption. Embedded systems used in these devices are facing energy shortage that leads designers to spread power electronic converters to achieve dynamic voltage and frequency scaling [Zhao]. Wherever it is possible, the linear low-drop converter is replaced by inductive DC-DC converters and/or capacitive DC-DC converters in order to improve the whole efficiency of the system. Since then the demand on power converters for portable electronic devices has attracted great interest [Sugawara]. Efficiency and footprint (or volume) are the main design criteria to ensure respectively a large operating range and a smaller device. These applications use switching mode power supply (SMPS) or inductive DC-DC converter which typically require the following characteristics: 1 W, V_{IN}=3.6 V, V_{OUT}=1 V, I_{OUT}=1 A. Passive components fill a significant part of the chip area occupied by power converters, even when the components are optimized for minimum area. Thus, for this power range, System-In-Package (Fig. 1) is more appropriate than monolithic integration (also named System-On-Chip).

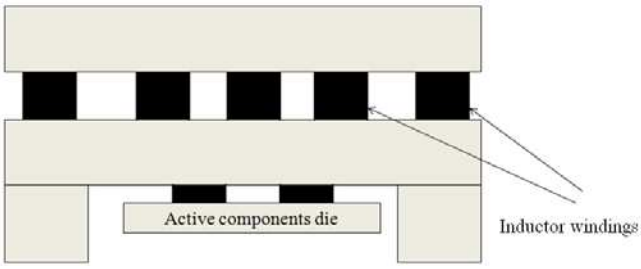

Fig. 1. Hybrid integration of System-In-Package

However, System-In-Package applications are still facing miniaturization issues due to passive components size [Musunuri]. Therefore, by increasing the switching frequency of DC-DC converters in the 10 MHz - 100 MHz frequency range [Chesneau], the size of filter passive components is dramatically reduced. Thus, the area devoted to passive components can be reduced below the 10 mm^2 range. In this condition, and for a typical 1 W DC-DC converter, the inductance value targeted for the output filter passive component is about 25 nH.

Since the system will be placed in a low-profile package, a planar inductor structure is preferred. Moreover, planar devices offer several advantages like better thermal management and higher power density.

Although research on planar inductors is concentrated on integrating air core inductors on silicon wafers [Wang], the application of ferrite magnetic substrates to planar inductors enables to increase the inductance value without increasing the stray capacitance between the coils and the ground plane. In our application, surface area is the key point of designing the inductor since the aim is to integrate the inductor on the top of a SMPS die in a surface area of 3mm^2.

This paper deals with a design methodology starting with Finite Element Method (FEM) simulation based on Flux2D simulator. The design aspect and boundary conditions will be presented and a specific figure of merit (MHz/mΩ.mm^2) will be proposed to evaluate our inductor performance targeting the DC-DC converter application. Next, the fabrication process using electroplating technique will be detailed. Finally, micro-fabricated inductors will be presented and their measured characteristics will be shown in the last section.

2. Context

Passive (inductor and capacitor) components have a major role in switching mode power supply since they ensure filtering function. However, they can occupy up to 30 per cent of the volume of the system. In such converter, current and voltage waveforms are far from sinusoidal. For example in a buck converter, voltage and current waveforms applied on the output inductor are square and triangular respectively. In this application, the output inductor is used to decrease the output current ripple defined as follows:

$$\Delta I_L = \frac{\alpha(1-\alpha)\cdot V_E}{L\cdot F} \tag{1}$$

where (L) is the inductance value, (F) represents the switching frequency, (V_E) is the input voltage, and (α) represents the duty cycle. Therefore, by increasing the frequency, the current ripple can be kept constant with a lower inductance value. For 1W – 1A DC-DC converter and 100 MHz switching frequency, an inductance value can be estimated at 30 nH. This inductor can be manufactured using coreless technology but it would require a large footprint area. Hence, the use of a magnetic material will allow fabricating the inductor with the same inductance value on a smaller surface area.

Since the inductor will be located as near as possible of the power and command circuit, electromagnetic interferences (EMI) must be limited using a magnetic circuit. Fig. 2 describes a qualitative magnetic field distribution in 3 cases: (a) coreless inductor (without magnetic material), (b) single layer (bottom side) and (c) double layer of ferrite magnetic

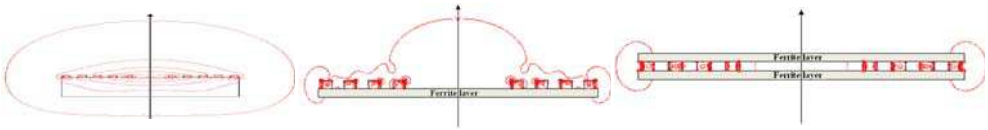

(a) (b) (c)

Fig. 2. Qualitative magnetic field distribution in: (a) coreless inductor (without magnetic material); (b) single layer (bottom side) and (c) double layer of ferrite magnetic material

material. We can observe in Fig.2 (b) and (c) that the magnetic field is confined within the magnetic material and thus electromagnetic disturbances are reduced.

Considering a low current ripple, which depends on the inductance value computed at the switching frequency, the current flow in the inductor could be considered equal to its average value. That is why direct current is the main contributor to losses in the windings and thus specific geometrical parameters for the winding must be optimized to reduce Joule effect losses at low frequency.

Inductance values at 100 MHz and DC resistance are computed using finite element method. Details are presented in the section below.

3. Design methodology

3.1 Finite Element Method (FEM) simulation

The design and analysis of the electromagnetic behaviour of magnetic components require finite element method software since analytical formulas are not available for the inductance and magnetic field calculation.

Based on finite element method, three-dimensional (3D) structures like the square planar inductor described in Fig. 3 require lots of memory, and computation time becomes impractical since high density meshing is required. Since commonly guidelines indicate that density meshing depends on skin effect in all materials, a frequency increase imply both a higher density mesh and computation time increase. This technique cannot be used in the design process.

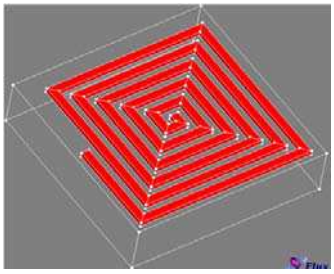

Fig. 3. 3D representation of a square planar inductor

Despite the three-dimensional form for such structure, we can assume a geometrical approximation to simplify our study. This approach consists in modifying the 3D structure by changing rectangular conductors to circular and concentric circles. Assuming this approximation, an axial symmetry appears as shown in Fig. 4.

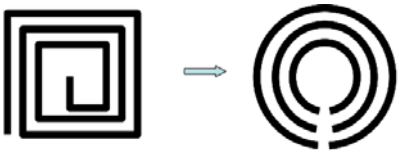

Fig. 4. Description of the geometrical approximation

Assuming these approximations, the planar inductor will be modelled in two-dimensional space as depicted in Fig. 5, which will allow to speed-up simulation. Therefore, the impact of geometrical parameters can be evaluated.

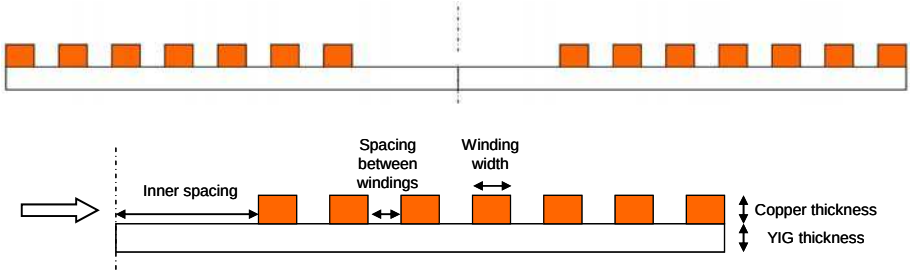

Fig. 5. Simplified 2D inductor representation

Fig. 5 describes the model dimensions and geometrical parameters. The number of turns, the turn width, the spacing between turns, the inner spacing, the magnetic substrate thickness (in this article we have used Yttrium Iron Garnet (YIG) as magnetic substrate) and copper thickness are taken into account. Simulations are performed with Flux2D® software. Regarding the inductor description, only the conductor cross-sections and magnetic substrate thickness will be described on the inductor half section. Boundary conditions applied for the magnetic field are tangential and capacitive behaviour will be neglected for frequency below 1 GHz [Yue].

An equivalent R-L circuit can be computed as depicted in Fig. 6. The impacts of both the geometry and frequency changes are observed on the magnetic field variation. Resistance and inductance values are calculated from active (P) and reactive (Q) power respectively as follow:

$$R = \frac{P}{I_{RMS}{}^2} \qquad L = \frac{Q}{\omega \cdot I_{RMS}{}^2} \tag{2}$$

where R is the inductor resistance, and I_{RMS} is the RMS current value, and ω is the angular frequency.

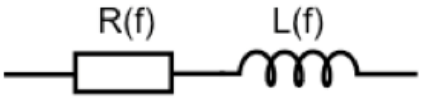

Fig. 6. Equivalent R-L circuit of the inductor

To evaluate the influence of geometrical parameters, we have considered a piecewise linear B-H curve for the magnetic material. In the linear region, a constant relative permeability is set to 25 while in the saturation region the flux density is below 0,25 T and relative permeability is equal to 1. Magnetic saturation and relative permeability are determined from characterization as described in section 3.2. Copper is also considered as a pure material of resistivity $1{,}7.10^{-8}$ Ω.m. Skin effect is taken into consideration as it contributes to increasing series resistance of the inductor at high frequency.

The choice of the frequency is important to compute resistance and inductance values. In many applications, the quality factor (Q) is commonly used to evaluate the AC performance of a structure. In such application, current and voltage waveforms are sinusoidal and the frequency of both signal is used according to equ (2).

$$Q = \frac{L\omega}{R} \tag{3}$$

As presented in the section 2, current and voltage waveforms are far from sinusoidal. Since the inductor is designed for reducing current ripple, the inductor excitation current waveform has a considerable DC component. Thus the inductor DC resistance is the main contributor to losses. On the other hand, the inductance value at switching frequency (100 MHz) will be computed to evaluate the current ripple.

In our application, a specific Merit Factor (equ (4)) taking into account DC resistance (R), inductance value (L) and footprint (S) is proposed to compare different models [Martin] and to evaluate a good power inductor performance.

$$MF = \frac{L_{100MHz}(nH)}{R_{DC}(m\Omega)\cdot S\left(mm^2\right)} \tag{4}$$

The following guidelines have been deduced from this parametric study:

- YIG doubles inductance value compared to an air core inductor with the same winding and reduces electromagnetic interferences. Moreover, simulations have also shown that increasing YIG thickness above 200 µm has only a slight effect on the inductance value.
- Copper thickness has a very small effect on inductance, but it contributes to a lower DC resistance.
- Increasing the space between the turns lowers the interwinding magnetic coupling, and thus decreases the inductance value.
- Widening the conductors reduces the inductance value, but it has an overall positive effect on Merit factor due to R_{DC} decreasing more significantly.
- Inductance value increases with the number of turns, but Merit Factor remains constant. This can be explained by the fact that improvement of MF is slowed down by the increase of the series resistance.
- Narrowing the inner spacing implies increasing the negative magnetic coupling and hence lowering the inductance value.

Simulations allowed evaluating our design with the optimal geometry contributing to the highest Merit Factor with taking into consideration the limitations of the technology parameters. Subsequently, we designed a planar spiral inductor of 3 mm^2 surface area (maximum surface area allowed in the converter).The inductor has four turns with a turn

width of 75 µm, a 75 µm spacing between the turns, an inner diameter of 200 µm and a conductor thickness of 50 µm. The inductance value targeted is 30 to 40 nH with a series resistance as low as possible. The copper thickness and width are constrained to the maximum resolution of the dry film photoresist. The magnetic material which also serves as a mechanical support has a thickness of 500 µm. Though, the inductor design exhausted the theoretical limits.

3.2 Magnetic material characterization

Two specific test benches have been set up in order to characterize the properties of magnetic materials. Both tests require a toroidal shaped material in order to deduce magnetic properties from electrical quantities with geometric characteristics of the core. Material characteristics (relative permeability μ_R and magnetic saturation B_{SAT}) obtained are used in the FEM simulations.

3.2.1 Hysteresis graph

B-H curves are measured using a hysteresis graph curve recorder developed in our lab using a transformer approach. The bench used is shown in Fig. 7. Inner and outer diameters of the sample are quite equal in order to assume a homogeneous field in the core. Hysteresis graph is used to measure B-H cycles (minor and major loops) for frequency up to 20 kHz.

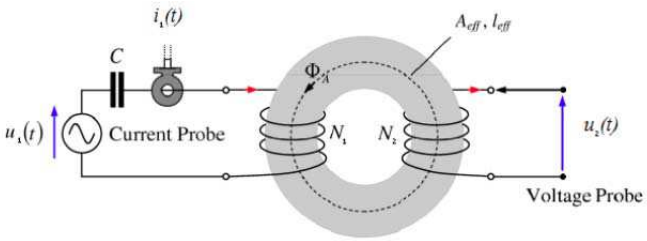

Fig. 7. Principle of B-H measurement

Magnetic field is imposed by the primary winding and is computed from the current. Flux density is obtained using induced voltage at the secondary winding. Starting from Ampere law presented in equ (5), magnetic field can be deduced from the current in the primary winding as described in equ (6). Flux density can be computed from equ (7). This method is used at low frequencies. The maximum frequency is estimated thanks to the equation of the skin depth.

$$\oint_{l_{eff}} \vec{H} \cdot \vec{dl} = \sum_{i=1}^{n} N_i \cdot i_i \tag{5}$$

$$H(t) = \frac{N_1}{l_{eff}} \cdot i_1(t) \tag{6}$$

$$B(t) = \frac{1}{A_{eff} \cdot N_2} \cdot \int u_2(t) \cdot dt \tag{7}$$

N_1 and N_2 represent the number of turns in primary and secondary side.

l_{eff} and A_{eff} are geometrical characteristics, the average length and section respectively of the toroidal sample.

Several ferrite materials have been tested and compared to datasheet. Since magnetic properties of ferrite material are not affected by machining, ring shape samples of YIG material have been machined from a ferrite plate. Fig. 8 shows B-H curve measured at 25 °C ambient temperature and for 1 kHz sinusoidal field excitation. Saturation induction is equal to 0.2 T and can be observed for a magnetic excitation beyond 200 A/m.

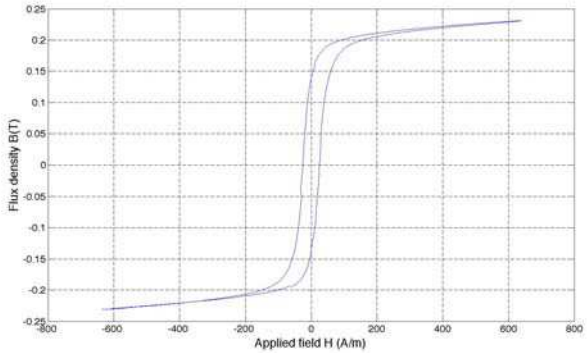

Fig. 8. Example of B-H curve

Permeability of the material can be deduced from the previous B-H cycle by using equ (8). However, this characterization method is not well adapted for high frequency. Complex permeability will be determined from impedance measurement presented in section 3.2.2.

$$\mu_{r_h} = \frac{1}{\mu_0} \cdot \left. \frac{\partial B}{\partial H} \right|_{H=h} \tag{8}$$

3.2.2 Impedance measurement

Permeability in the alternating-current magnetic field is defined as complex relative permeability ($\mu_{complex}$). The real part of the complex relative permeability (μ') represents the amount of energy stored in the magnetic material from alternating-current magnetic field. On the other hand, the imaginary part (μ'') indicates energy loss to the alternating-current magnetic field. Complex relative permeability can be computed from impedance measurement (equ 9).

$$\mu_{complex} = -j \cdot \frac{\underline{Z} \cdot l_{eff}}{2 \cdot \pi \cdot f \cdot \mu_0 \cdot S} = \mu' - j \cdot \mu'' \tag{9}$$

Impedance analyzer Agilent 4294A associated with the dedicated adapter for magnetic material characterization (Agilent 16454A) are used and permeability measurement can be performed in a wider frequency range (40 Hz – 110 MHz) (Fig. 9). The measurement respects the setup described in the manual guide and recommended by the manufacturer.

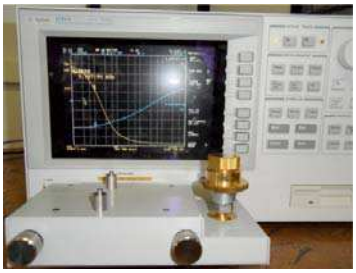

Fig. 9. Impedance meter Agilent 4294A and magnetic module

Characterizations have been performed on a toroidal shaped sample of YIG material in the 100 kHz – 110 MHz frequency range. Complex impedance (module and phase) is shown in Fig. 10. From this measurement, complex relative permeability has been computed using equ (9) and exhibited in Fig. 11. A behaviour change can be observed from 3 MHz with the change of the slope. This change can be explained by the permeability variation as described in Fig. 11.

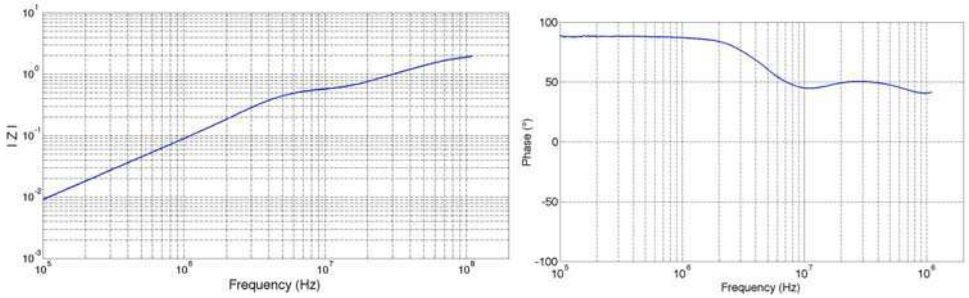

Fig. 10. Module (left) and phase (right) of the impedance

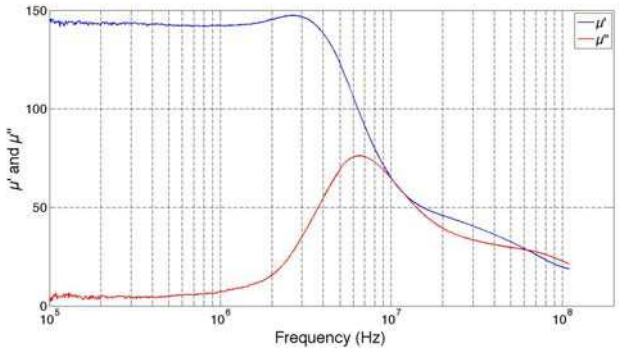

Fig. 11. Complex relative permeability (μ′ and μ′′)

Results detailed in Fig. 11 have good adequacy with the literature [Kedous] [Siblini]. Up to 3 MHz the real part of the permeability is quite constant and equal to 140 and decreases for higher frequencies. At high frequencies, the magnetic field is non-uniform and diffuses in the material which implies a permeability decrease. This phenomenon depends on the

angular frequency (ω), material resistivity (ρ) and permeability (μ). It can be estimated with the expression of the skin depth (δ) (equ. 10). This decrease in permeability reaches 25 for 100 MHz.

$$\delta = \sqrt{\frac{2 \cdot \rho}{\omega \cdot \mu}} \tag{10}$$

This test bench allowed the computation of the permeability in a wide frequency range. The low excitation level permits to identify μ' (the real part of the permeability) in order to fill in the simulation parameters.

4. Technological process

At 100 MHz switching frequency, the inductance value required is small and the integration of the inductor on the SIP using micro-fabrication techniques may be practical. Although significant previous work has been done on integrated micro-fabricated inductors for power conversion applications [Fukuda, Prabhakaran, Gao], much of this work has focused on the frequency range of less than 10 MHz. To be practical, the micro-inductor technology must be implemented in a cost effective manner which normally depends on the size of the component and the number of steps used in the fabrication. Thus, the electroplating technique, a low temperature and a simple technique is used to deposit thick copper conductors and hence allowing to minimize DC resistance with high current handling (1 A). In comparison to [Orlando], a higher inductance to DC resistance ratio was achieved in a relatively large area and with a relatively more complex process. Other techniques can be used but they present several technological disadvantages (complexity; high temperature process, cost). Sputtering technique was used in [Nakazawa] to deposit a thin layer of magnetic material. This technique is not cost effective since it allows low deposition rate (1-2 microns per hour) and is highly dependent on temperature. Sputtering technique can also be used to deposit the conductor lines but also presents the same inconvenient. Although copper can be deposited by using chemical vapor deposition (CVD) [Pan] or electroless [Jiang, Schacham-Dtamand] but electroplating remains the main technique for depositing thick copper conductors because it Provides a higher deposition rate than other methods, good ductility and high adhesion at low temperature in a simple and low cost manner [Bunshah].

In this section, we detail the fabrication process. In order to electroplate the copper windings, a metallic thin layer serving a double purpose as a conductive layer and with a relatively high adhesion to the magnetic substrate is deposited. Ti 500 Å /Cu 1500 Å seed layer is chosen to be deposited on the magnetic substrate using evaporation technique (Fig. 15). This choice allows minimizing the stress at the interface of the seed layer/electroplated copper due in particular to the difference in the CTE of the materials. The magnetic material used is a solid substrate with a thickness of 500 μm.

Dry film photoresist is then laminated and patterned using UV photolithography (Fig. 12, Fig. 16)). Dry film photoresist is an alternative solution for epoxy-based resin (SU-8,..) since it requires fewer number of technological steps to be processed.

Copper windings are deposited using electroplating technique (Fig. 17). This process is cost effective since it is simple to implement at ambient temperature (25 °C) and it allows us to

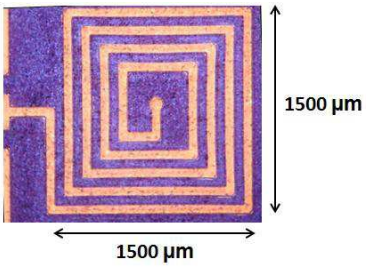

Fig. 12. Patterned inductor windings

reach a high thickness of copper in a reasonable time (copper deposition rate around 15 µm/h). Copper deposition is carried out in a horizontal cell (Fig. 13). Current densities used are in the 10-20 mA/cm² range (calculated for the active area on the sample). As a result, deposit height is uniform across the sample and electroplated copper shows a good crystalline quality.

After electroplating the copper windings, the remaining dry film is removed and the seed layer is wet etched to isolate the coil turns (Fig.14, Fig.17).

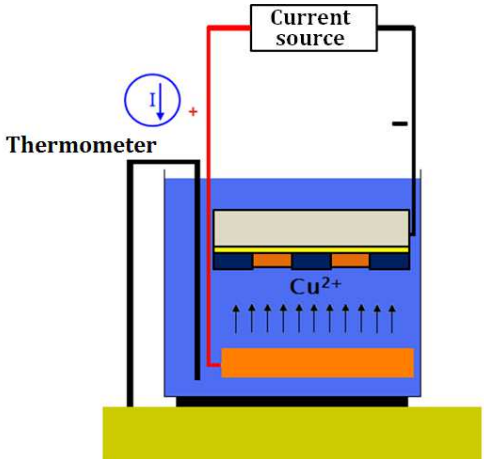

Fig. 13. Copper electroplating bench

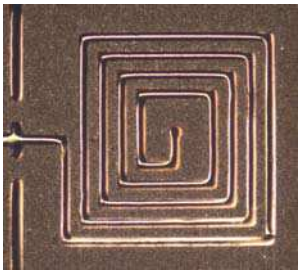

Fig. 14. Isolated inductor windings after dry film and seed layer removal

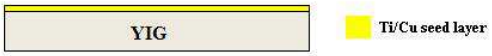

Fig. 15. Deposition of the Ti/Cu seed layer

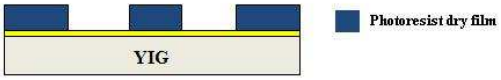

Fig. 16. Inductor windings patterning

Fig. 17. Copper electroplating to fill the molds

Fig. 18. Dry film and seed layer removal

5. Experimental results

Fig 19 shows SEM images of the fabricated micro-inductor fabricated. Inductors have a high aspect ratio : 75 µm in width and 50 µm in copper thickness sufficient to hold a 1 A current flow.

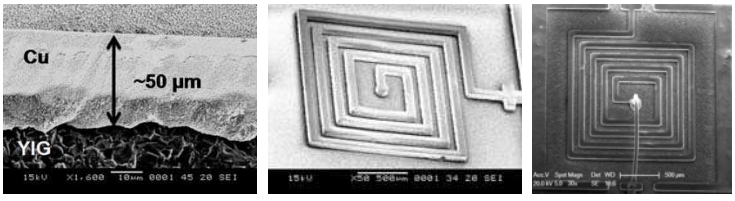

Fig. 19. SEM images of the micro-fabricated inductor

In order to perform electrical characterization, bonding has been realized (fig. 19 right) to connect the inner terminal to the external bump contact of the inductor. Device measurements have been carried out using a Vector Network Analyzer and Ground-Signal-Ground (GSG) probes from 10 MHz to 1GHz. Two-port scattering parameters (S-parameters) have been measured and then changed to admittance parameters (Y-parameters). Inductance L of the spiral inductor is subsequently computed from the resultant Y_{11} parameters after the bonding and the de-embedding procedure. Its expression is given by:

$$L = \frac{1}{\mathrm{Im}\,ag(Y_{11})} \cdot \frac{1}{2 \cdot \pi \cdot f} \tag{11}$$

Fig. 20 shows the simulated and measured inductance from 10 MHz to 1 GHz. Referring to equ.1, increasing the frequency with keeping the inductance value constant results in a lower current ripple and hence a satisfying voltage ripple. But since, the inductor will be integrated in a DC-DC converter with 100 MHz switching frequency, we are interested in the 100-200 MHz frequency range. Moreover, we measured an inductance value of 36 nH at 100 MHz. The perturbations at low frequency (10-50 MHz) are due to the fact that the vector network analyzer is expected to measure the s-parameters at higher frequencies. There is a 15% difference between the measured and simulated inductance value at 100 MHz because of the approximations done to perform 2D simulations. DC resistance was also measured using a Source Measuring Unit and we obtained a value of 20 mΩ (Fig. 5). Merit factor corresponding to our application is equal to 0,6 nH/mΩ.mm². Compared to [O'donnell], we have reached a higher Merit Factor for the inductor with the same number of turns and with a smaller area. In [Orlando], a higher inductance to DC resistance ratio was achieved but in a relatively large area of 5.6 x 5.6 mm² and with a relatively complex process. Thus our inductor design combined with a high permeability magnetic material allowed us to achieve good results compared to literature.

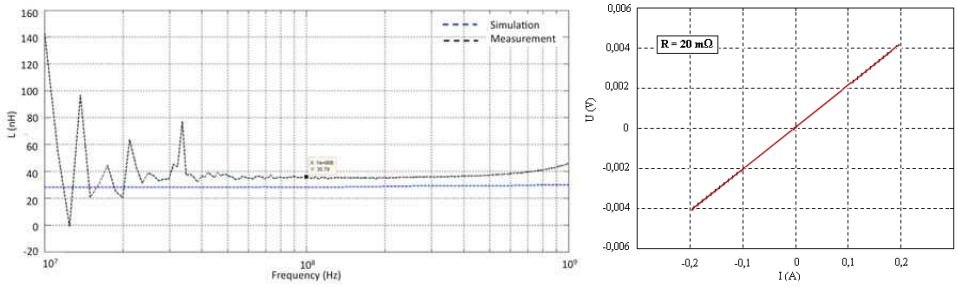

Fig. 20. Measured and simulated inductance (left) and measured DC resistance (right)

Impedance measurement is more appropriated in the 1kHz to 100 MHz frequency range. The development of this test bench is under progress.

6. Conclusions

The development of a DC-DC converter that can operate with switching frequency up to 100 MHz allows the integration of inductors since the inductance value required is low (≤ 50 nH). This implies a lower footprint and a lower profile compatible with hybrid integration for nomad applications.

This chapter presents the development of planar micro inductor using a ferrite magnetic material. A design methodology based on finite element method and dedicated software have been presented. According to geometrical approximations, a comparative study has been led to evaluate the influence of geometrical parameters. A design has been defined according to the inductor's specifications.

Magnetic properties of the magnetic material have been extracted from the hysteresis graph and impedance measurements in order to identify B-H loop and permeability, respectively. Based on these results, FEM simulations have been carried out and results were discussed. Merit Factor was presented respecting critical characteristic of integrated power inductor.

Planar spiral inductors were realized by electroplating technique. This technique and the fabrication process have been detailed. Advantages and limits have been shown. The inductors characterization have been carried out from 10 MHz to 1 GHz. Finally, simulation and characterization results have been compared with good adequacy.

7. References

J. Zhao, X. Dong, Y. Xie, "An energy-efficient 3D CMP design with fine-grained voltage scaling", Design, Automation & Test in Europe Conference & Exhibition, 14-18 March 2011.

S. Sugawara, A. Nakamori, Z. Hayashi, M. Edo, H. Nakazawa, Y. Katayama, M. Gekinozu, K. Matsuzaki, A. Matsuda, E. Yonezawa, K. Kuroki: "Characteristic of a monolithic dc–dc converter utilizing a thin-film inductor", Proc. IPEC, Tokyo, Japan, 2000.

S. Musunuri and P. L. Chapman, "Optimization issues for fully-integrated CMOS dc-dc converters," Proc. Conf. Record IEEE Industrial Applications Society Annu. Conf., 2002, pp. 2405–2410.

D. Chesneau, F. Hasbani, "Benefits and Constraints of SMPS Integration in Wireless Multi Media Terminals", 1st IEEE International Workshop on Power Supply on Chip (PwrSoC)", Cork, Sept. 21-24, 2008.

N. Wang, T.O'Donnell, S. Roy, P. McCloskey, S.C. O'Mathuna, "Micro-inductors integrated on Silicon for Power supply on chip", Journal of Magnetism & Magnetic Materials, 2007, vol. 316, n. 2, pp. 233-237.

C. P. Yue and S. S. Wong, "Physical modeling of spiral inductors on silicon", IEEE Trans. Electron Devices, vol. 47, no. 3, pp. 560–568, Mar. 2000.

C. Martin, B. Allard, D. Tournier, M. Soueidan, J.-J. Rousseau, D. Allessem, L. Menager, V. Bley, J. -Y. Lembeye, "Planar inductors for high frequency DC-DC converters using microwave magnetic material", IEEE ECCE, 2009, pp. 1890-1894.

A. Kedous-Lebouc, "Materiaux magnétiques en génie électriques 2", edition Lavoisier 2006, ISBN 2-7462-1461-X.

A.Siblini, I.Khalil, JP.Chatelon, JJ.Rousseau, "Determination of initial magnetic permeability of YIG thin films using the current sheet method", Advanced Materials Research, 2011, Vol. 324, pp. 290-293.

S. Prabhakaran, Y. Sun, P. Dhagat, W. Li and C. R. Sullivan, "Microfabricated V-Groove power inductors for high-current low-voltage fast-transient DC-DC converters", IEEE 36thPower Electronics Specialists Conference, 2005, PESC '05, pp.1513–1519.

Y. Fukuda, T. Inoue, T. Mizoguchi, S. Yatabe and Y. Tachi, "Planar inductor with ferrite layers for DC-DC converter", IEEE Transactions on Magnetics, Vol. 39, No. 4, July 2003, pp. 2057-2061

X. Gao, Y. Zhou, Wen Ding, Ying Cao, Chong Lei, Ji An Chen,and Xiao Lin Zhao, "Fabrication of ultralow-profile micromachined inductor with magnetic core material", IEEE Transactions On Magnetics, Vol. 41, No. 12, December 2005, pp. 4397-4400.

B. Orlando, R. Hida, R. Cuchet, M. Audoin, B. Viala, D. Pellissier-Tanon,X. Gagnard, and P. Ancey, "Low-resistance integrated toroidal inductor for power management", IEEE Transactions On Magnetics, Vol. 42, No. 10, October 2006, pp. 3374-3376.

H. Nakazawa, M. Edo, Y. Katayama, M. Gekinozu, S. Sugahara, Z.Hayashi, K. kuroki, E. Yonezawa, and K. Matsuzaki, "Micro-DC/DC converter that integrates planar

inductor on power IC", IEEE Transaction on Magnetics, Vol. 36, No. 5, September 2000, pp. 3518-3520.

T. Pan, A. Baldi, E. Davies-Venn, R. Drayton, and B. Ziaie, "Fabrication and modeling of silicon-embedded high-Q inductors", Journal of Micromechanics and Microengineering, Vol 15, 2005, pp. 849-854.

H. Jiang, Y. Wang, J. Yeh, and N. C. Tien, "On-Chip spiral inductors suspended over deep copper-lined cavities", IEEE Transactions on Microwave Theory and Techniques, Vol. 48, No. 12, December 2000.

Y. Shacham-Dtamand , V. M. Dubin, "Copper electroless deposition technology for ultra-large-scale integration (ULSI) metallization", Microelectronic Engineering 33 (1997) 47-58.

R. F. Bunshah, "Handbook of deposition technologies for films and coatings", ISBN: 0-8155-1337-2.

T. O'Donnell, N. Wang, R. Meere, F. Rhen, S. Roy, D. O'Sullivan, C. O'Mathuna, "Microfabricated inductors for 20 MHz DC-DC converters", APEC 2008. Twenty-Third Annual IEEE, February 2008, pp. 689-693.

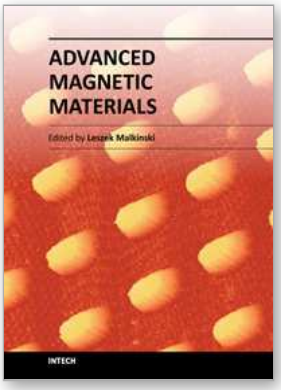

Advanced Magnetic Materials

Edited by Dr. Leszek Malkinski

ISBN 978-953-51-0637-1
Hard cover, 230 pages
Publisher InTech
Published online 24, May, 2012
Published in print edition May, 2012

This book reports on recent progress in emerging technologies, modern characterization methods, theory and applications of advanced magnetic materials. It covers broad spectrum of topics: technology and characterization of rapidly quenched nanowires for information technology; fabrication and properties of hexagonal ferrite films for microwave communication; surface reconstruction of magnetite for spintronics; synthesis of multiferroic composites for novel biomedical applications, optimization of electroplated inductors for microelectronic devices; theory of magnetism of Fe-Al alloys; and two advanced analytical approaches for modeling of magnetic materials using Everett integral and the inverse problem approach. This book is addressed to a diverse group of readers with general background in physics or materials science, but it can also benefit specialists in the field of magnetic materials.

How to reference

In order to correctly reference this scholarly work, feel free to copy and paste the following:

Elias Haddad, Christian Martin, Bruno Allard, Maher Soueidan and Charles Joubert (2012). Micro-Fabrication of Planar Inductors for High Frequency DC-DC Power Converters, Advanced Magnetic Materials, Dr. Leszek Malkinski (Ed.), ISBN: 978-953-51-0637-1, InTech, Available from: http://www.intechopen.com/books/advanced-magnetic-materials/micro-fabrication-of-planar-inductors-for-high-frequency-dc-dc-power-converter

INTECH
open science | open minds

InTech Europe
University Campus STeP Ri
Slavka Krautzeka 83/A
51000 Rijeka, Croatia
Phone: +385 (51) 770 447
Fax: +385 (51) 686 166
www.intechopen.com

InTech China
Unit 405, Office Block, Hotel Equatorial Shanghai
No.65, Yan An Road (West), Shanghai, 200040, China
中国上海市延安西路65号上海国际贵都大饭店办公楼405单元
Phone: +86-21-62489820
Fax: +86-21-62489821